Electronic Supplementary Material (ESI) for Nanoscale.
This journal is © The Royal Society of Chemistry 2021

Supplementary Information to:
Fast-response photogating in monolayer MoS_2 phototransistors

*Daniel Vaquero[1], Vito Clericò[1], Juan Salvador-Sánchez[1], Elena Díaz[2], Francisco Domínguez-Adame[2], Leonor Chico[2,3], Yahya M. Meziani[1], Enrique Diez[1] and Jorge Quereda[1]**

[1] Nanotechnology Group, USAL–Nanolab, Universidad de Salamanca, E-37008 Salamanca, Spain

[2] GISC, Departamento de Física de Materiales, Universidad Complutense, E-28040 Madrid, Spain

[3] Instituto de Ciencia de Materiales de Madrid, CSIC, E-28049 Madrid, Spain

* e-mail: j.quereda@usal.es

Table of contents

S1. Room-temperature measurements

S2. Photocurrent spectroscopy

S3. Extended discussion on power dependence of PCE

S4. Estimation of carrier density and Fermi energy shift

S5. Raman and photoluminescence characterization

S6. Optical image of the device

S7. Derivation of photoconductive gain

S1. Room-temperature measurements

In this section we present photocurrent measurements at room temperature, analogous to the low-temperature measurements showed in the main text.

Supplementary Figure S1a shows a room temperature photocurrent spectrum acquired at $V_g - V_{th} = -10$ V with a power density of 1 mW cm^{-2}, as well as its fit to a quintuple Lorentzian, corresponding to the five main exciton transitions described in the main text (T_A, X_{1s}^A, T_B, X_{1s}^B and X_{2s}^A). Due to the thermal energy, the peaks of the spectrum are broadened and red-shifted in comparison with the low temperature photocurrent spectrum presented in Supplementary Section 2.

Supplementary Figure S1b shows the transfer curve of the device at $V_{ds} = 10$ V. As expected, the increase in the current near the threshold voltage is here less abrupt than at low temperature.

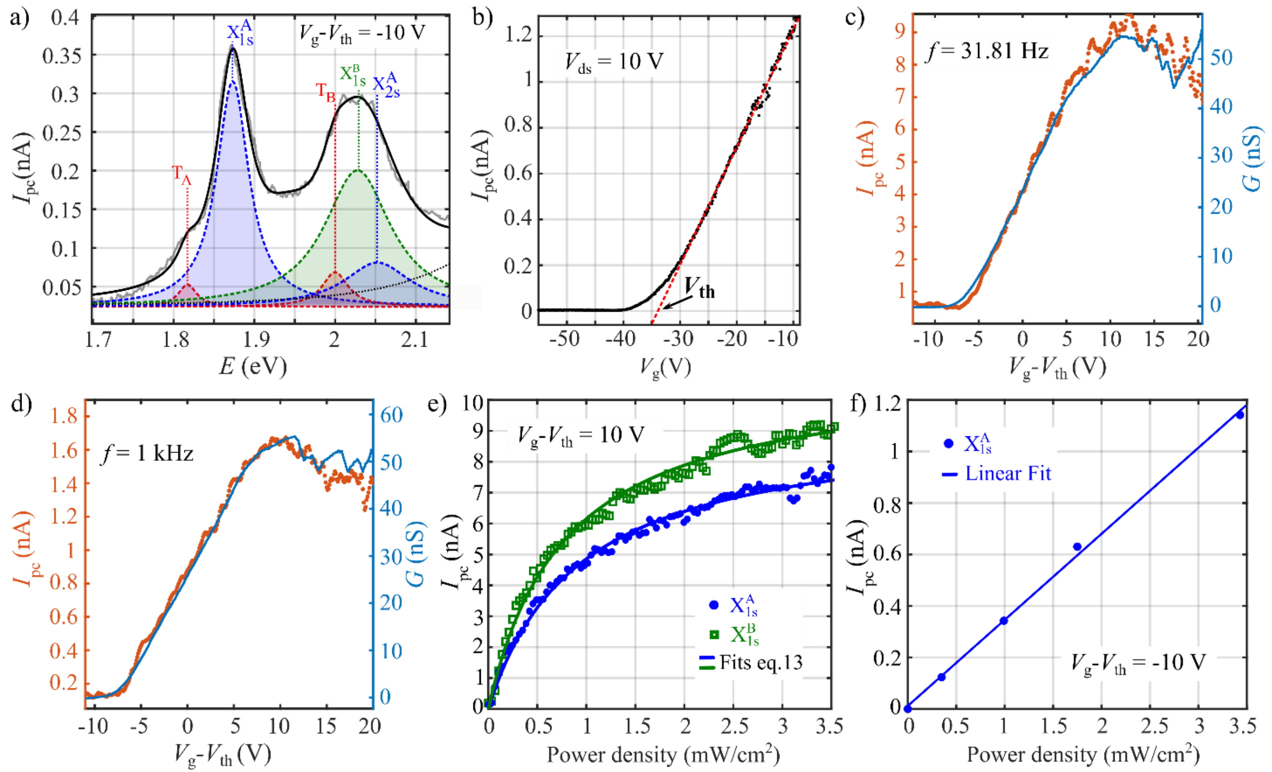

Supplementary Figure S1- Room temperature photocurrent measurements. (a) Photocurrent spectrum of the 1L-MoS2 phototransistor (gray solid line) and multi-lorentzian fitting (black solid line). The five main transitions are depicted in the figure. (b) Transfer curve of the device in dark at room temperature and V_{ds}=10V. (c-d) Gate dependence of the photocurrent depicted with the transconductance of the device in resonance with the exciton A at different frequencies of modulation (c) f = 31.81 Hz and (d) f = 1kHz. (e) Power dependence of the photocurrent at Vg-Vth=10V in resonance with the exciton A and B. The solid lines correspond to the fittings of the data to eq. 13. (f) Power dependence of the photocurrent at V_g-V_{th} = – 10 V, in resonance with the exciton A.

Supplementary Figures 1c and 1d show the photocurrent as a function of the gate voltage V_g for illumination at E=1.87 eV and two different light-modulation frequencies: $f = 31.81$ Hz (c) and $f = 1$ kHz (d). Consistently with the results and the theoretical model presented in the main text, the photocurrent is strongly correlated with the transconductance of the device regardless of the modulation frequency. It is worth remarking that, for the room-temperature measurements presented here, the photocurrent measured at low modulation frequency is roughly 8 times larger than the one measured at 1 kHz, indicating that the effect of slow-responding traps due to polar adsorbates is much stronger at room temperature than at $T = 5$ K.
Finally, Supplementary Figure S1e shows the power dependence of the photocurrent at $V_g - V_{th} = 10$ V, for two different illumination energies, matching the A and B exciton transitions, E=1.87 eV and E=2.01 eV respectively. The illumination power dependence of I_{PC} is sublinear, as expected for the photogating effect. Similarly to our results at low temperature, the illumination power dependence of I_{PC} becomes linear for gate voltages below the threshold voltage (see Supplementary Figure S1f), indicating that for this regime, the photoconductivity is dominated by the photoconductive effect.

S2. Photocurrent spectroscopy

Supplementary Figure S2 shows a photoconductivity spectrum of our device acquired for $V_{ds} = 10\,\mathrm{V}$, and $V_g - V_{th} = -30\,\mathrm{V}$. At low temperature the main excitonic spectral features can be clearly resolved, with bandwidths as low as 8 meV.[1] The spectrum presents two main peaks corresponding to the A and B neutral excitons (X_{1s}^{A} and X_{1s}^{B} respectively), as well as three smaller features corresponding to the trion states (T^{A} and T^{B}) and the 2s excited state X_{2s}^{A} of the A exciton. Detailed information on the experimental setup for photocurrent spectroscopy, as well as an in-depth analysis of the spectral features in 1L-MoS_2 transistors can be found in ref. 1. The sample is placed inside a pulse-tube cryostat (T = 5 K) and the whole device is exposed to laser illumination through an optical access. For illumination we use a SuperK Compact supercontinuum laser from NKT photonics, and the excitation wavelength is selected by an Oriel MS257 monochromator (1200 lines/mm). Using this light source allows us to scan the spectral range from 450 nm to 840 nm. The excitation signal is modulated by an optical chopper and the photocurrent is registered by a lock-in amplifier.

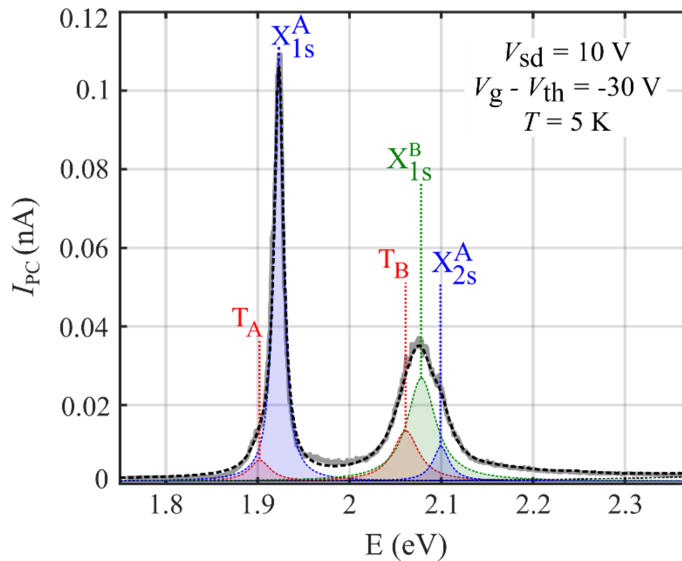

Supplementary Figure S2. Low-temperature photocurrent spectrum of the encapsulated 1L-MoS_2 device.

S3. Extended discussion on power dependence of PCE

In the main text (equation 10) we obtained an expression for the increase of photoconductivity caused by the photoconductive effect (PCE):

$$\Delta\sigma_{\mathrm{PCE}} = q(\mu_{\mathrm{n}} + \mu_{\mathrm{p}})p_{\mathrm{ph}} + q\mu_{\mathrm{p}}p_{\mathrm{t}}, \tag{1}$$

Replacing p_{ph} and p_{t} by their expressions (equations 8 and 9 in the main text) we get:

$$\Delta\sigma_{\mathrm{PCE}} = q\tau_{\mathrm{r}}(\mu_{\mathrm{n}} + \mu_{\mathrm{p}})\phi_{\mathrm{A}} + q\mu_{\mathrm{p}}\frac{\phi_{\mathrm{A}}D_{\mathrm{t}}\tau_{r}}{\phi_{\mathrm{A}}\tau_{\mathrm{r}} + D_{\mathrm{t}}\left(\frac{\tau_{\mathrm{t}}}{\tau_{\mathrm{d}}}\right)}, \tag{2}$$

The first term in the right-hand side of equation (2) is linear with the power (note that $\phi_{\mathrm{A}} \propto P_{\mathrm{D}}$). Thus, in absence of trap states, *i.e.* for $D_{\mathrm{t}} = 0$, $\Delta\sigma_{\mathrm{PCE}}$ is linear with the power (as long as the main relaxation mechanism is Shockley-Read-Hall recombination). When a finite density of traps is present, it is useful to consider the three following situations:

(i) $\phi_{\mathrm{A}} \gg D_{\mathrm{t}}\frac{\tau_{\mathrm{t}}}{\tau_{\mathrm{r}}\tau_{\mathrm{d}}}$

This is the relevant scenario illumination power densities large enough for the trap states to become saturated. Under this situation, the second right-hand term in equation (2) can be simplified as

$$\frac{q\mu_{\mathrm{p}}\phi_{\mathrm{A}}D_{\mathrm{t}}\tau_{r}}{\phi_{\mathrm{A}}\tau_{\mathrm{r}} + D_{\mathrm{t}}\left(\frac{\tau_{\mathrm{t}}}{\tau_{\mathrm{d}}}\right)} \approx q\mu_{\mathrm{p}}D_{\mathrm{t}}\,, \tag{3}$$

which gives only a constant contribution to $\Delta\sigma_{\mathrm{PCE}}$. Thus, the total photoconductivity remains linear with the power:

$$\Delta\sigma_{\mathrm{PCE}} \approx q\tau_{\mathrm{t}}(\mu_{\mathrm{n}} + \mu_{\mathrm{p}})\phi_{\mathrm{A}} + q\mu_{\mathrm{p}}D_{\mathrm{t}}, \tag{4}$$

(ii) $\phi_{\mathrm{A}} \ll D_{\mathrm{t}}\frac{\tau_{\mathrm{t}}}{\tau_{\mathrm{r}}\tau_{\mathrm{d}}}$

For very low illumination power, the density of available trap states only changes by a very small amount due to light exposure. Under this situation, the second right-hand term in equation (2) can be again simplified as

$$\frac{q\mu_{\mathrm{p}}\phi_{\mathrm{A}}D_{\mathrm{t}}\tau_{r}}{\phi_{\mathrm{A}}\tau_{\mathrm{r}} + D_{\mathrm{t}}\left(\frac{\tau_{\mathrm{t}}}{\tau_{\mathrm{d}}}\right)} \approx q\mu_{\mathrm{p}}\frac{\tau_{\mathrm{d}}\tau_{\mathrm{r}}}{\tau_{\mathrm{t}}}\phi_{\mathrm{A}}\,, \tag{5}$$

which now gives a linear contribution to $\Delta\sigma_{\mathrm{PCE}}$. Again, the total photoconductivity remains linear with the power:

$$\Delta\sigma_{\mathrm{PCE}} \approx \left(q\tau_{\mathrm{t}}\left(\mu_{\mathrm{n}}+\mu_{\mathrm{p}}\right)+q\mu_{\mathrm{p}}\frac{\tau_{\mathrm{d}}\tau_{\mathrm{r}}}{\tau_{\mathrm{t}}}\right)\phi_{\mathrm{A}}\,, \tag{6}$$

In this scenario, the effect of localized states is to enhance the slope of $\Delta\sigma_{\mathrm{PCE}}$ while keeping it linear with the power density.

(iii) $\phi_{\mathrm{A}} \approx D_{\mathrm{t}}\frac{\tau_{\mathrm{t}}}{\tau_{\mathrm{r}}\tau_{\mathrm{d}}}$

Finally, for intermediate power densities, equation (2) cannot be simplified and the presence of localized states results in a sublinear contribution to photocurrent.

S4. Estimation of carrier density and Fermi energy shift

Note: The measurements presented in this article were performed in the same device studied in an earlier publication by the authors[1]. This supplementary section is reprinted from the Supplementary Information of the mentioned publication for convenience of the readers.

In the following we use a capacitor model to estimate the increase in carrier density δn produced by the gate voltage. The gate voltage V_g, *i.e.* the total voltage drop between the Si back gate and the MoS_2 channel, will be given by

$$\delta V_g = \delta E \cdot d + \frac{1}{e}\delta E_F \tag{7}$$

Where E is the electric field between the electrode and the flake, $-e$ is the electron charge and E_F is the Fermi energy. For a parallel plate with two different insulator layers the geometrical capacitance is

$$C_g = \left(\frac{d_{SiO_2}}{\epsilon_0 \epsilon_{SiO_2}} + \frac{d_{BN}}{\epsilon_0 \epsilon_{BN}}\right)^{-1}, \tag{8}$$

and we have

$$\delta E \cdot d = \frac{e\delta n}{C_g}. \tag{9}$$

Replacing in (S8) and using $\delta E_F = (\delta E_F/\delta n)\ \delta n = \delta n/D$, where D is the density of states of the 2D semiconductor, we get

$$\delta V_g = \frac{de}{\epsilon_0 \epsilon_d} \cdot \delta n + \frac{1}{eD}\delta n = \left(\frac{1}{C_g} + \frac{1}{C_q}\right) e\delta n\,, \tag{10}$$

where we have defined the quantum capacitance as $C_q = e^2 D$. We can now express equation (10) in terms of the Fermi energy using $\delta E_F = \delta n/D$. We get

$$\delta V_g = \left(\frac{1}{C_g} + \frac{1}{C_q}\right) eD\ \delta E_F = \left(\frac{1}{C_g} + \frac{1}{C_q}\right)\frac{C_q}{e}\ \delta E_F\,. \tag{11}$$

Therefore, solving for E_F, we have

$$\delta E_F = \frac{e\delta V_g}{1 + \frac{C_q}{C_g}}\ . \tag{12}$$

We model the density of states of 1L-$MoSe_2$ as the step function

$$D(E) = \begin{cases} g_{2D} \equiv \dfrac{\mu_{\mathrm{eff}}}{\pi \hbar^2} & \text{if } E > E_{\mathrm{CB}} \\ 0 & \text{if } E > E_{\mathrm{CB}} \end{cases} , \tag{13}$$

where μ_{eff} is the electron effective mass in MoS_2 ($\mu_{\mathrm{eff}} = 0.35\, m_0$) and E_{CB} is the edge of the conduction band. Then, by integrating equation (12) we get

$$\Delta E_{\mathrm{F}} = \frac{e}{1 + \frac{e^2 g_{2\mathrm{D}}}{C_{\mathrm{g}}}} \left(V_{\mathrm{g}} - V_{\mathrm{th}}\right) , \tag{14}$$

where V_{th} is the threshold voltage at which $E_{\mathrm{F}} = E_{\mathrm{CB}}$. In our case, we get $\Delta E_{\mathrm{F}}/(V_{\mathrm{g}} - V_{\mathrm{th}}) = 0.28\ \mathrm{meV\,V^{-1}}$, which for the maximal gate voltages applied here ($V_{\mathrm{g}} - V_{\mathrm{th}} = 50\mathrm{V}$) gives $\Delta E_{\mathrm{F}} = 14\ \mathrm{meV}$. Finally, the density of excess carriers, n can be obtained as $n = \Delta E_{\mathrm{F}} \cdot g_{2\mathrm{D}} = 7.17 \times 10^{10} \mathrm{cm^{-2} V^{-1}} (V_{\mathrm{g}} - V_{\mathrm{th}})$. Thus, the maximal carrier densities reached here are of $n = 3.58 \times 10^{12} \mathrm{cm^{-2}}$.

S5. Raman and photoluminescence characterization

Note: The measurements presented in this article were performed in the same device studied in an earlier publication by the authors[1]. This supplementary section is reprinted from the Supplementary Information of the mentioned publication (with minor changes) for convenience of the readers.

We determine the thickness of the MoS_2 flakes used for device fabrication by a combination of optical microscopy, Raman mapping and photoluminescence. Supplementary Figure S3a shows an optical microscope image of the MoS_2 flake used to fabricate the device described in the main text, and Supplementary Figure S3b shows a false color map of the ratio between the summed intensities of the A_{1g} + E^1_{2g} Raman peaks of MoS_2 and the intensity of the Si peak, in logarithmic scale. The different thicknesses can be clearly distinguished in the figure. Supplementary Figure S3c shows individual spectra acquired at the different regions labelled in Supplementary Figure S3a. The number of layers can be here confirmed by the difference between the spectral positions of the E^1_{2g} and A_{1g} peaks, Δf.[2,3] For the thinnest region we obtain $\Delta f = 19.4\ \mathrm{cm}^{-1}$, compatible with the values given in literature for 1L-MoS_2.

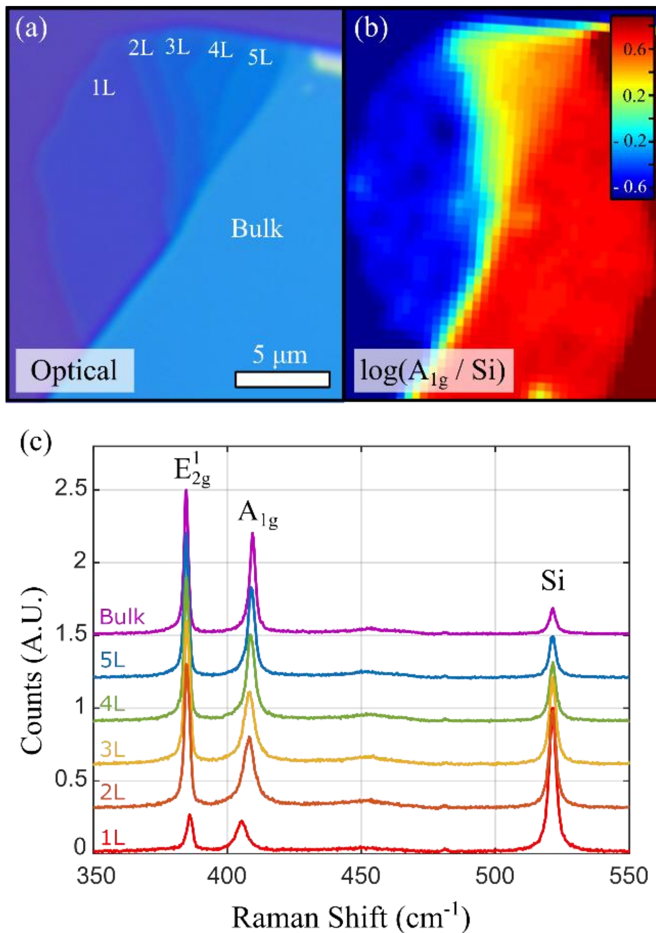

Supplementary Figure S3. Raman characterization of the MoS_2 thickness. (a) Optical microscopy image of the MoS_2 flake used for the device of the main text. The labels indicate regions with different thickness. (b) False color Raman map of the difference between the A_{1g} and Si peak intensities, as labeled in panel c. (c) Raman spectra acquired at the different regions labelled in Figure 1a. The spectra show three prominent peaks corresponding to the A_{1g} and E^1_{2g} Raman modes of MoS_2 and the Si Raman mode.

We further confirm the thickness of the MoS_2 flakes by measuring the position of the A exciton peak in their photoluminescence spectrum. Supplementary Figure S4 shows a room-temperature photoluminescence spectrum acquired at the monolayer MoS_2 flake. The X_{1s}^{A} exciton peak can be clearly observed at around 1.87 eV, in good agreement with the values found in literature.[3–5]

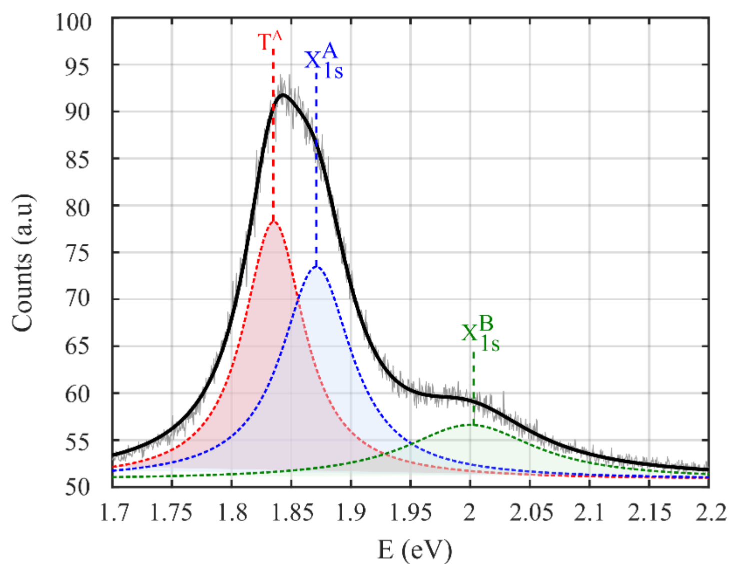

Supplementary Figure S4. Room-temperature photoluminescence spectra of monolayer MoS_2 on SiO_2 under 530 nm excitation. The dashed lines are the individual contributions from the TA, X_{1s}^{A} and X_{1s}^{B} exciton transitions.

S6. Optical image of the device

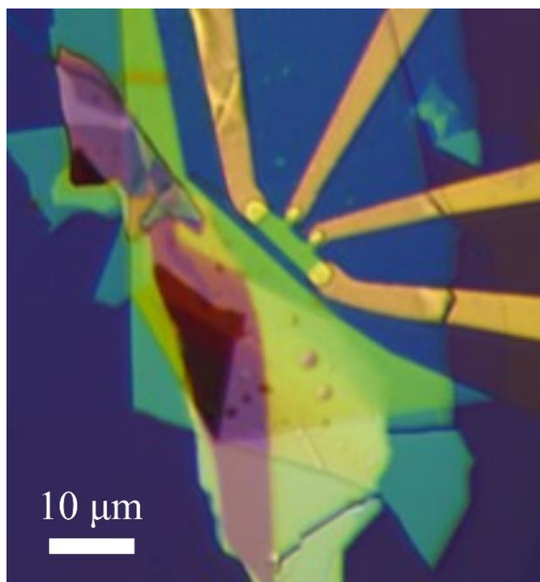

Supplementary Figure S5. Optical image of the encapsulated 1L-MoS_2

S7. Derivation of photoconductive gain

It can be convenient in some cases to express the device's photoresponse in terms of the photoconductive gain G_{ph}. This quantity is defined as the ratio between the number of charge carriers collected by the electrodes and the number of absorbed photons:

$$G_{ph} = \frac{\text{collected charge carriers}}{\text{absorbed photons}} = \frac{q^{-1} I_{\text{PC}}}{\phi_{\text{A}} W L} \tag{155}$$

where q is the elementary charge, and W and L are the width and length of the semiconductor channel, respectively.

In a trap-free semiconductor, in absence of photogating effect, the photoconductive gain can be obtained as [6]

$$G_{ph} = \frac{\tau_{\text{r}}}{\tau_{\text{tr,n}}} + \frac{\tau_{\text{r}}}{\tau_{\text{tr,p}}} \tag{166}$$

where τ_{r} is the electron-hole recombination lifetime and $\tau_{\text{tr,n}}$ ($\tau_{\text{tr,p}}$) is the transit time for electrons (holes), *i.e.* the time required for an electron (hole) to drift across the semiconductor channel, from the source to the drain electrode.

Let us now derivate the expression of G_{ph} in the presence of shallow states such as the ones considered in the main text. To do so, it results convenient to separate I_{PC} into its photoconductive (ΔI_{PCE}) and photogating (ΔI_{PGE}) contributions. For ΔI_{PCE}, combining equations 2 and 3 of the main text we have

$$\Delta I_{\text{PCE}} = \frac{\text{W}}{\text{L}} V_{\text{ds}} q \left(\mu_{\text{n}} n_{\text{ph}} + \mu_{\text{p}} p_{\text{ph}} \right). \tag{17}$$

Assuming a uniform electric field E across the channel, we can write $V_{\text{ds}} = EL$. Then, reordering terms we have

$$\Delta I_{\text{PCE}} = qWL \left(\frac{E\mu_{\text{n}}}{L} n_{\text{ph}} + \frac{E\mu_{\text{p}}}{L} p_{\text{ph}} \right) = qWL \left(\frac{E\left(\mu_{\text{n}} + \mu_{\text{p}}\right)}{L} p_{\text{ph}} + \frac{E\mu_{\text{p}}}{L} p_{\text{t}} \right). \tag{18}$$

Equation 18 can now be rewritten in terms of the electron and hole transit times $\tau_{\text{tr,n}} = L/E\mu_{\text{n}}$ and $\tau_{\text{tr,p}} = L/E\mu_{\text{p}}$. This yields

$$\Delta I_{\text{PCE}} = qWL \left(p_{\text{ph}} \left(\frac{1}{\tau_{\text{tr,n}}} + \frac{1}{\tau_{\text{tr,p}}} \right) + \frac{p_{\text{t}}}{\tau_{\text{tr,p}}} \right). \tag{19}$$

We now replace p_{ph} and p_{t} by their expressions from equations 9 and 10 of the main text:

$$\Delta I_{\text{PCE}} = qWL\left(\phi_{\text{A}}\tau_{\text{r}}\left(\frac{1}{\tau_{\text{tr,n}}} + \frac{1}{\tau_{\text{tr,p}}}\right) + \frac{\tau_r}{\tau_{\text{tr,p}}}\,\frac{\phi_{\text{A}}D_{\text{t}}}{\phi_{\text{A}}\tau_{\text{r}} + D_{\text{t}}\left(\frac{\tau_{\text{t}}}{\tau_{\text{d}}}\right)}\right). \tag{19}$$

Finally, using equation 15 for the photoconductive gain we get

$$G_{\text{ph,PCE}} = \frac{q^{-1}\Delta I_{\text{PCE}}}{\phi_{\text{A}}WL} = \frac{\tau_{\text{r}}}{\tau_{\text{tr,n}}} + \frac{\tau_{\text{r}}}{\tau_{\text{tr,p}}} + \frac{\tau_r}{\tau_{\text{tr,p}}}\,\frac{\phi_{\text{A}}D_{\text{t}}}{\phi_{\text{A}}\tau_{\text{r}} + D_{\text{t}}\left(\frac{\tau_{\text{t}}}{\tau_{\text{d}}}\right)}. \tag{20}$$

For ΔI_{PGE} equation 14 in the main text gives

$$I_{\text{PGE}} = \frac{D_{\text{t}}}{\beta}\frac{dI_{\text{ds}}}{dV_{\text{g}}}\frac{1}{1 + \frac{D_{\text{t}}}{\phi_{\text{A}}\tau_r}\left(\frac{\tau_{\text{t}}}{\tau_{\text{d}}}\right)}, \tag{21}$$

Which corresponds to a photoconductive gain of

$$G_{\text{ph,PGE}} = \frac{D_{\text{t}}}{qWL\beta}\frac{dI_{\text{ds}}}{dV_{\text{g}}}\frac{1}{\phi_{\text{A}} + \frac{D_{\text{t}}}{\tau_r}\left(\frac{\tau_{\text{t}}}{\tau_{\text{d}}}\right)}, \tag{22}$$

The total photoconductive gain in the device will be the sum of the two contributions:

$$G_{\text{ph}} = G_{\text{ph,PCE}} + G_{\text{ph,PGE}} \tag{23}$$

$$G_{\text{ph}} = \frac{\tau_{\text{r}}}{\tau_{\text{tr,n}}} + \frac{\tau_{\text{r}}}{\tau_{\text{tr,p}}} + \left(\frac{\phi_{\text{A}}\tau_r}{\tau_{\text{tr,p}}} + \tau_r\frac{1}{qWL\beta}\frac{dI_{\text{ds}}}{dV_{\text{g}}}\right)\frac{D_{\text{t}}}{\phi_{\text{A}}\tau_{\text{r}} + D_{\text{t}}\left(\frac{\tau_{\text{t}}}{\tau_{\text{d}}}\right)}, \tag{24}$$

Thus, the presence of shallow traps results in an increase in the photoconductive gain, compared to the trap-free situation. Note that, if the density of trap states is set to zero, $D_{\text{t}} = 0$, the third term in the right-hand side of equation 24 cancels out, and we recover the expression of G_{ph} for a trap-free scenario (equation 15).

Bibliography

1 D. Vaquero, V. Clericò, J. Salvador-Sánchez, A. Martín-Ramos, E. Díaz, F. Domínguez-Adame, Y. M. Meziani, E. Diez and J. Quereda, *Commun. Phys.*, , DOI:10.1038/s42005-020-00460-9.

2 H. Li, Q. Zhang, C. C. R. Yap, B. K. Tay, T. H. T. Edwin, A. Olivier and D. Baillargeat, *Adv. Funct. Mater.*, 2012, **22**, 1385–1390.

3 M. Buscema, G. a. Steele, H. S. J. van der Zant and A. Castellanos-Gomez, *Nano Res.*, 2014, **7**, 1–50.

4 A. Splendiani, L. Sun, Y. Zhang, T. Li, J. Kim, C.-Y. Chim, G. Galli and F. Wang, *Nano Lett.*, 2010, **10**, 1271–5.

5 J. W. Christopher, B. B. Goldberg and A. K. Swan, *Sci. Rep.*, 2017, **7**, 1–8.

6 H. Fang and W. Hu, *Adv. Sci.*, , DOI:10.1002/advs.201700323.